International Journal of Thermal Sciences 48 (2009) 1978–1987

Contents lists available at ScienceDirect

International Journal of Thermal Sciences

journal homepage: www.elsevier.com/locate/ijts

Entropy generation in turbulent natural convection due to internal heat generation

Sheng Chen [a,b,*], Manfred Krafczyk [b]

[a] State Key Lab of Coal Combustion, Huazhong University of Science and Technology, Wuhan 430074, China
[b] Institute for Computational Modeling in Civil Engineering, Technical University, Braunschweig 38106, Germany

ARTICLE INFO

Article history:
Received 31 August 2008
Received in revised form
12 February 2009
Accepted 13 February 2009
Available online 18 March 2009

Keywords:
Entropy generation
Turbulent natural convection
Internal heat generation
Lattice Boltzmann method

ABSTRACT

In this study numerical predictions of entropy generation in turbulent natural convection due to internal heat generation in a square cavity are reported for the first time. Results of entropy generation analysis are obtained by solving the entropy generation equation. The values of velocity and temperature, which are the inputs of the entropy generation equation, are obtained by an improved thermal lattice-BGK model proposed in this paper. The analyzed range is wide, varying from the steady laminar symmetric state to the fully turbulent state. Distributions of entropy generation numbers, for various Rayleigh numbers, Prandtl numbers, and Eckert numbers, are given.

1. Introduction

Natural convection occurring in nature and many industrial devices are driven by internal heating [1,2], ranging from the mantle convection in the Earth [3,4] to the cooling of a molten nuclear reactor core [5,6]. Natural convection due to internal heat generation has been lately receiving increasing attention because of its relevance to nuclear safety issues [5–8]. As discussed in Refs. [6,8], an inadequate or prolonged absence of nuclear reactor core cooling may cause core melting to occur in a light water reactor. The core debris may heat up on account of the volumetric decay heat generation to form a molten pool in natural convection. Consequently, to predict the behavior of the convectional flow and to optimally design the thermal systems are necessary in the nuclear engineering [6,9].

The pioneers on this subject are Kulacki and his collaborators, who conducted several experiments using Joule heating as a volumetric heat source [10,11]. In these experiments, which were primarily applicable to the nuclear industry, heat transfer through a horizontal fluid layer was assessed for different boundary cooling arrangements. Asfia et al. conducted experiments of natural convection in a spherical cavity [12]. The working fluid was Freon-113, which was heated with microwaves. The range of the Rayleigh number (Ra) tested was between 2×10^{10} and 1.1×10^{14} at the Prandtl (Pr) number 8. Recently, Lee et al. studied high modified Rayleigh number natural convection with the aid of the simulant internal gravitated material apparatus rectangular pool [6]. The modified Ra based on the power input was varied from 10^9 to 10^{14}. The Pr of working fluid ranged from 4 to 8 for water, and 0.7 for air. In their work, particular attention was paid to the influence of Pr on natural convection heat transfer in the pool. The relation between the Nusselt number (Nu) and the modified Ra was determined for different boundary conditions in the rectangular pool.

However, it is still a challenge for experiments to capture the turbulent flow motion at high Ra. In fact, the highest Ra attainable in an apparatus of a given size is usually quite limited for a fluid such as water. Because of the unknown properties of the core melt at high temperatures, the researchers were unable to reproduce adequate accident conditions. Moreover, it is not a simple task to measure Pr dependence in convectional turbulence by experiments. Therefore, numerical simulations are required to predict the turbulent flows especially at very high Ra [7,8]. In Ref. [9], the effect of the Pr on the Nu distributions for different geometries was demonstrated. In their work, Ra spanned from 10^6 to 10^{12} and Pr from 0.6 to 7. The authors found that the influence of Pr is small in convection-dominated regions and much more significant in

* Corresponding author at: Institute for Computational Modeling in Civil Engineering, Technical University, Braunschweig 38106, Germany.
E-mail addresses: chen@irmb.tu-bs.de (S. Chen), kraft@irmb.tu-bs.de (M. Krafczyk).

1290-0729/$ – see front matter © 2009 Elsevier Masson SAS. All rights reserved.
doi:10.1016/j.ijthermalsci.2009.02.012

Nomenclature

c	particle speed
C	Smagorinsky constant
D	effective thermal diffusivity
$\vec{u}$	fluid velocity vector
$\vec{e}_k$	discrete velocity
F_k, G_j	source terms in Eqs. (7) and (21)
$\vec{g}$	gravity
g_k, f_j	distribution function for velocity and temperature field
g_k^{eq}, f_j^{eq}	equilibrium distribution function for velocity and temperature field
H	height of simulation domain
$\vec{v}$	equilibrium velocity vector
p	pressure
Nu	Nusselt number
Ec	Eckert number
Pr	Prandtl number
Be	Bejan number
Ra	Rayleigh number
$\phi_{\alpha\beta}$	strain rate tensor
S_{total}	total entropy generation number
S	entropy generation number
T	simulation time interval
L_b	length of the boundary
$\vec{x}$	phase space

Greek symbols

Δx, Δy	grid spacing in x and y direction
Δt	time step
Θ	dimensionless temperature
ν	effective kinematic viscosity
μ	effective dynamic viscosity
τ_u	relaxation time for velocity
τ_Θ	relaxation time for temperature
ρ	density
α	thermal diffusivity
ω_k, χ_k	the weights for equilibrium distribution function
Δ	filter width
φ	irreversibility distribution ratio

Subscripts and superscripts

D	thermal
μ	viscous
j, k	discrete velocity direction
0	initial index
-	filter operator or average
t	turbulent
α, β	spatial index
Ω, T	global, total

conduction-dominated regions. Regardless, the influence of the Pr on fluid behavior grows with the increase of the Ra. Dinh and Nourgaliev reviewed the turbulence modeling in large volumetrically heated liquid pools [13]. The attention was focused on different k–ϵ models as well as on Reynolds stress models. Wörner et al. made a comprehensive study of turbulence in an internally heated convective fluid layer using direct numerical simulation [14]. The Pr was 7 and the Ra in the range of 10^5–10^9. The authors showed that the k–ϵ models are not suitable for the simulation of turbulent natural convection with internal heat generation. In order to save computational resources with the time-consuming direct numerical simulation, they had to initiate from a parabolic temperature profile and to stop before an overall thermal equilibrium being achieved. Recently, Horvat et al. pointed out that such way would lead to a severe underprediction of overall heat transfer over the simulation domain [8]. And they proposed a large-eddy model as a remedy [8]. The simulations were carried out at Ra of 10^6–10^{11} and Pr between 0.25 and 0.6. The newest report can be found in Ref. [5], which focused on transient turbulent natural convection heat transfer from a volumetric energy generating source placed inside a cylindrical enclosure filled with low Pr number fluid ($Pr = 0.005$).

Despite the significant differences in their appearances and technical details, numerical models employed in previous studies almost are based on the solution of the Navier–Stokes-type equations. These methods rest on the spatial and temporal discretizations of the macroscopic equations. During the past two decades, a mesoscopic method, the lattice Boltzmann method (LBM) has matured as an efficient alternative and promising numerical scheme for simulating and modeling complicated physical systems [15–18]. Unlike the conventional numerical methods based on discretizations of macroscopic continuum equations, the LBM is based on microscopic models and mesoscopic kinetic equations for fluids. The kinetic nature of LBM enables itself very suitable for fluid systems [17]. Especially, the LBM has been compared favourably with the spectral method [19], the artificial compressibility method [20], the finite volume method [21,22] and finite difference method [23]. All quantitative results further validate excellent performances of the LBM not only in computational efficiency but also in numerical accuracy [24]. Using the LBM to simulate two dimensional turbulent natural convection due to internal heat generation was firstly conducted by Shi et al. [25]. The simulations were carried out at $10^6 \leq Ra \leq 10^{12}$ and Pr between 0.25 and 0.6. Recently Liu et al. developed an improved large-eddy-based thermal lattice Boltzmann model for such turbulent natural convection [7]. They simulated the natural convection flow with internal heat generation in a square cavity with $Ra = 10^6 - 10^{13}$ and $Pr = 0.25 - 0.6$.

As is seen, all of the studies in the above cited literature, there is no study that is conducted to analyze entropy generation in turbulent natural convection due to internal heat generation, although it has been demonstrated that the entropy generation analysis is a powerful tool for optimal design of thermal systems [26–34]. The purpose of this study is twofold: The first one is to

Table 1
Time-boundary-averaged Nusselt number $Nu_{T,\,b}$ with different grid resolutions.

Ra		256×256	512×512
10^6	a	12.6300	12.6300
	b	6.3352	6.3351
	c	10.4603	10.6983
10^7	a	20.4309	20.4309
	b	7.1514	7.2550
	c	15.6576	15.1810
10^8	a	28.2318	28.2320
	b	8.7980	8.7981
	c	22.9925	22.0424
10^9	a	42.3476	42.3479
	b	11.1717	11.4835
	c	35.7966	34.1332

Note. a, $Nu_{T,\,b}$ at the top wall; b, $Nu_{T,\,b}$ at the bottom wall; c, $Nu_{T,\,b}$ at the left wall.

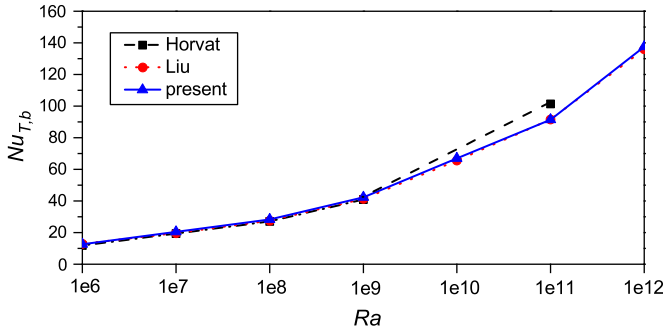

Fig. 1. Rayleigh number vs time-boundary-averaged Nusselt number on the top boundary.

investigate the behaviors of local and total entropy generation rates in turbulent natural convection due to internal heat generation. In order to obtain the necessary macro-quantities, such as temperature and velocity, which are the inputs for the entropy generation analysis, a unified improved thermal large-eddy-based lattice Boltzmann model is designed following the line of our previous work [35]. The models proposed in Refs. [7,25] can be derived from the present model. Furthermore the nonphysical effects of the models in Refs. [7,25] are canceled in the present model. To the best knowledge of the present author, this is the first attempt to combine the LBM and the entropy generation analysis to study a complex thermal system, which is the second purpose of the present study.

2. Governing equations

The thermal flow is governed by the unsteady Boussinesq equations which read [7,8,25]

$$\nabla\cdot\vec{u} = 0 \tag{1}$$

$$\frac{\partial\vec{u}}{\partial t} + \vec{u}\cdot\nabla\vec{u} = -\nabla p + \nu\Delta\vec{u} + \vec{g}\beta(\Theta-\Theta_0) \tag{2}$$

$$\frac{\partial\Theta}{\partial t} + \vec{u}\cdot\nabla\Theta = \alpha\Delta\Theta + I \tag{3}$$

where ρ, p and α are the density, the pressure and the thermal diffusivity of working fluid, respectively. H is the length of the

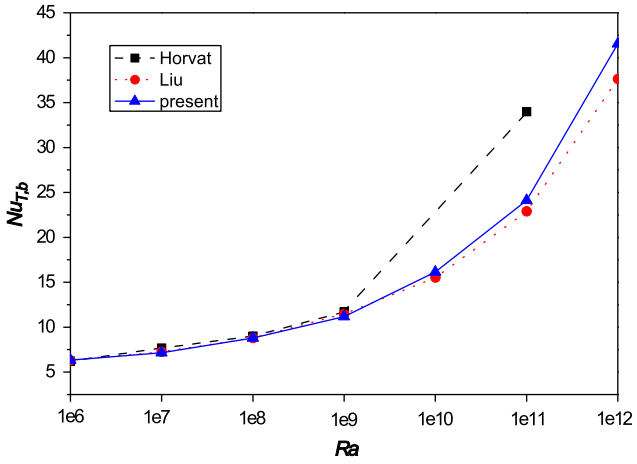

Fig. 2. Rayleigh number vs time-boundary-averaged Nusselt number on the bottom boundary.

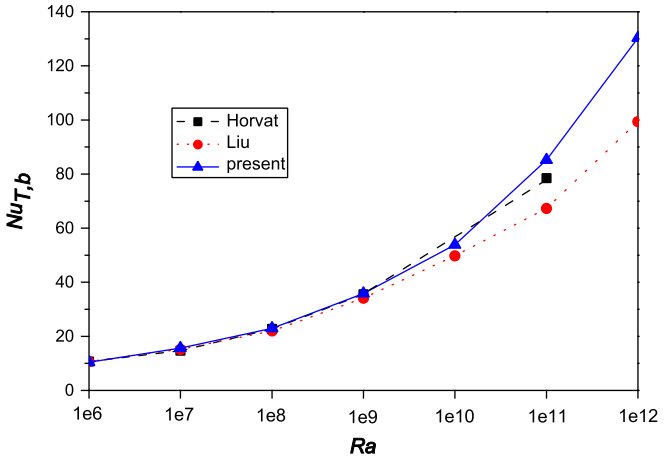

Fig. 3. Rayleigh number vs time-boundary-averaged Nusselt number on the left boundary.

domain. The gravity $\vec{g}$ downward. The Rayleigh number is defined as $Ra = c_p\rho g\beta I H^5/\alpha^2\nu$, where I is the volumetric heat generation; c_p is the specific heat and Θ is the temperature dilatation.

With the aid of the normalizing characteristic quantities, i.e. length with H, velocity with $(\alpha/H)Ra^{0.5}$, pressure with $\rho(\alpha/H)^2Ra$, temperature with $(\Theta-\Theta_0)/\Delta\Theta$ and time with $H^2/\alpha Ra^{-0.5}$, the corresponding dimensionless equations read [7,8,5]

$$\nabla\cdot\tilde{\vec{u}} = 0 \tag{4}$$

$$\frac{\partial\tilde{\vec{u}}}{\partial t} + \tilde{\vec{u}}\cdot\nabla\tilde{\vec{u}} = -\nabla\tilde{p} + \tilde{\nu}\Delta\tilde{\vec{u}} + Pr\tilde{\Theta}\frac{\vec{g}}{|\vec{g}|} \tag{5}$$

$$\frac{\partial\tilde{\Theta}}{\partial t} + \tilde{\vec{u}}\cdot\nabla\tilde{\Theta} = \tilde{D}\Delta\tilde{\Theta} + \tilde{D} \tag{6}$$

where $\tilde{\nu} = PrRa^{-0.5}$, $\tilde{D} = Ra^{-0.5}$. For simplification, the tilde, which denotes dimensionless quantities, is omitted in the rest part. A detailed description of the normalizing procedure could be found in Ref. [25].

3. Unified lattice Boltzmann model

3.1. Flow field

The evolution equation for the flow field reads

$$g_k(\vec{x}+c\vec{e}_k\Delta t, t+\Delta t) - g_k(\vec{x},t) = -\tau_u^{-1}\left[g_k(\vec{x},t) - g_k^{(eq)}(\vec{x},t)\right] + \Delta t F_k \tag{7}$$

where $\vec{e}_k$ is the discrete velocity direction. $c = \Delta x/\Delta t$ is the fluid particle speed. Δx, Δt and τ_u are the lattice grid spacing, the time step and the dimensionless relaxation time for the flow field respectively. The force term F_k must satisfy

$$\sum_{k\geq 0} F_k = 0, \sum_{k\geq 0} F_k\vec{e}_k = \vec{F} \equiv Pr\Theta\frac{\vec{g}}{|\vec{g}|} \tag{8}$$

As Guo et al. demonstrated [36], the form of F_k must be chosen appropriately to recover correct equations of hydrodynamics. In the present model, the force term F_k is given as

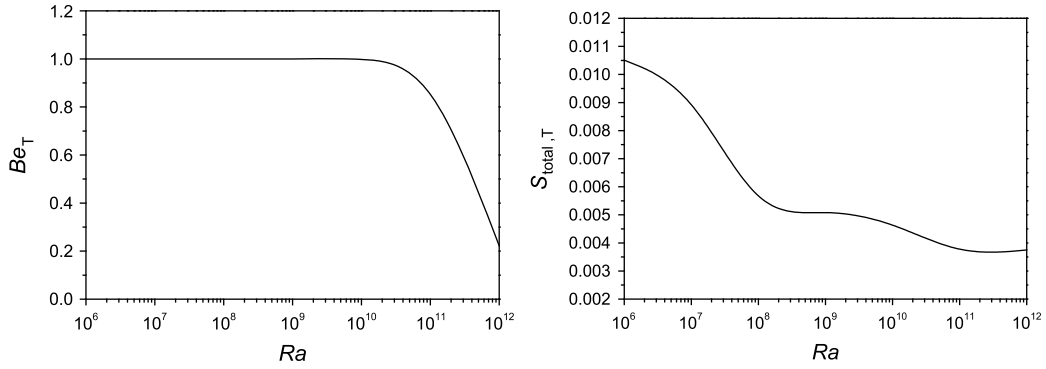

Fig. 4. Time-volume-averaged Bejan number and time-averaged total entropy generation number vs Rayleigh number, $Pr = 0.6$ and $Ec = 10^{-10}$.

$$F_k = \omega_k\left(1-\frac{1}{2\tau_u}\right)\left[\frac{c\vec{e}_k\cdot\vec{F}}{c_s^2}+\frac{(c\vec{e}_k\cdot\vec{v})(c\vec{e}_k\cdot\vec{F})}{c_s^4}-\frac{\vec{v}\cdot\vec{F}}{c_s^2}\right] \tag{9}$$

c_s is the speed of sound and the equilibrium velocity $\vec{v}$ is defined as

$$\vec{v} = \sum_{k\geq 0} c\vec{e}_k g_k + \frac{\Delta t}{2}\vec{F} \tag{10}$$

It should be pointed out that the forms of $\vec{v}$ and F_k used in Refs. [7,25] would produce nonphysical terms of order $O(\nabla\cdot\vec{F})$ and $O(\nabla\cdot(\vec{F}\,\vec{u}))$ in the continuum equation and the momentum equation respectively [36,37], although the magnitudes of these nonphysical terms are very small in most previous simulations [36–38].

$g_k(\vec{x},t)$ is the distribution function at node $\vec{x}$ and time t with velocity $\vec{e}_k$, and $g_k^{(eq)}(\vec{x},t)$ is the corresponding equilibrium distribution. The equilibrium distribution in the present model is defined by

$$g_k^{(eq)} = \chi_k p + s_k \tag{11}$$

where

$$s_k = \omega_k\left[\frac{c\vec{e}_k\cdot\vec{v}}{c_s^2}+\frac{(c\vec{e}_k\cdot\vec{v})^2}{2c_s^4}-\frac{|\vec{v}|^2}{2c_s^2}\right] \tag{12}$$

the parameter χ_k is determined by the moment constraints [35], which lead

$$\chi_{k|(k\neq 0)} = \omega_k/c_s^2, \quad \chi_{k|(k=0)} = (\omega_0-1)/c_s^2 \tag{13}$$

the values of ω_k for one-, two- and three-dimensional problems can be found in Ref. [17].

The effective kinematic viscosity is determined by

$$\nu = (\tau_u - 0.5)c_s^2\Delta t \tag{14}$$

and ν can be split into two parts:

$$\nu = \nu_0 + \nu_t \tag{15}$$

where ν_0 is the initial kinetic viscosity, and the turbulent eddy viscosity ν_t is obtained by [7,8]

$$\nu_t = (C\Delta)^2\left(|\bar{\phi}|^2+\frac{Pr}{Pr_t}\nabla\Theta\cdot\frac{\vec{g}}{|\vec{g}|}\right)^{1/2} \tag{16}$$

The first term in Eq. (16) represents stress forces while the second term represents buoyancy. The constant C is called the Smagorinsky constant and is adjustable. In the present study, we take $C = 0.1$ and the turbulent Prandtl number Pr_t is set to 0.4, which are identical with that in Ref. [7]. And Δ is the filter width [8]. $|\bar{\phi}|$ is the magnitude of the large scale strain rate tensor

$$|\bar{\phi}| = \sqrt{2\bar{\phi}_{\alpha\beta}\bar{\phi}_{\alpha\beta}} \tag{17}$$

where $\bar{\phi}_{\alpha\beta} = (\partial_\alpha\bar{u}_\beta + \partial_\beta\bar{u}_\alpha)/2$, and the over bar indicates filtered values. In the next section we will show in detail how to obtain the value of $|\bar{\phi}|$ through the LBM because this term will also be used in entropy generation calculation. After some tedious algebraic operations one can get:

$$\tau_u = \tau_0 + \frac{(C\Delta)^2}{c_s^2\Delta t}\left(|\phi|^2+\frac{Pr}{Pr_t}\nabla\Theta\cdot\frac{\vec{g}}{|\vec{g}|}\right)^{1/2} \tag{18}$$

where $\tau_0 = \nu_0/(c_s^2\Delta t) + 0.5$.

The velocity and pressure are given by

$$\vec{u} = \sum_{k\geq 0} c\vec{e}_k g_k + \frac{\Delta t}{2}\vec{F} \tag{19}$$

$$p = \frac{c_s^2}{1-\omega_0}\left[\sum_{k\neq 0} g_k + s_0(\vec{u})\right] \tag{20}$$

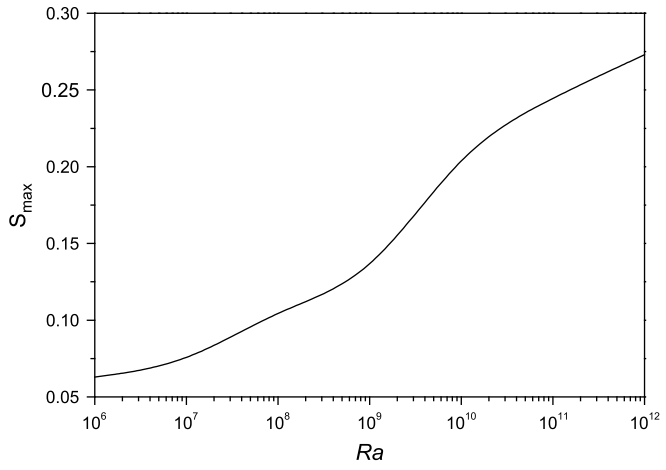

Fig. 5. The maximum of entropy generation number vs Rayleigh number, $Pr = 0.6$ and $Ec = 10^{-10}$.

3.2. Temperature field

The evolution equation for the temperature field reads

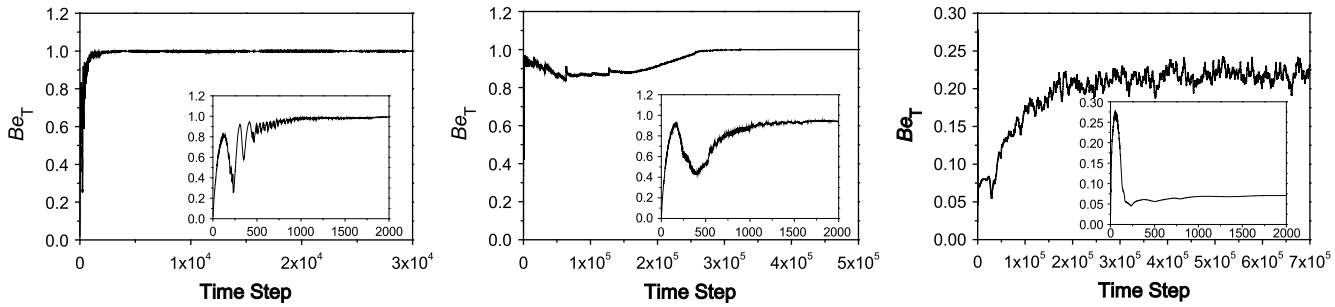

Fig. 6. Variation of time-volume-averaged Bejan number versus time step: $Ra = 10^6$(left), $Ra = 10^9$(center) and $Ra = 10^{12}$(right) with $Pr = 0.6$ and $Ec = 10^{-10}$.

$$f_j(\vec{x}+c\vec{e}_j\Delta t, t+\Delta t) - f_j(\vec{x},t) = -\tau_\Theta^{-1}\left[f_j(\vec{x},t) - f_j^{(eq)}(\vec{x},t)\right] + \Delta t G_j \tag{21}$$

where τ_Θ is the dimensionless relaxation time for temperature field and

$$f_j^{(eq)} = \frac{\Theta}{b}\left[1 + b\frac{\vec{e}_j\cdot\vec{u}}{2c}\right] \tag{22}$$

$$G_j = \frac{D}{b}\left[1 + b\frac{\vec{e}_j\cdot\vec{u}}{2c}\right] \tag{23}$$

where b is the number of discrete velocity directions for the temperature field [39,40]. The temperature Θ is obtained in terms of the distribution function by

$$\Theta = \sum_j f_j \tag{24}$$

The effective thermal diffusivity D is given by

$$D = 2c^2(\tau_\Theta - 0.5)\Delta t/b \tag{25}$$

Similar as ν, the effective thermal diffusivity D also can be split into two parts:

$$D = D_0 + D_t \tag{26}$$

D_0 is the initial thermal diffusivity. The turbulent thermal diffusivity $D_t = \nu_t/Pr_t$. And

$$\tau_\Theta = \tau_{\Theta_0} + \frac{bD_t}{2c^2\Delta t} \tag{27}$$

where $\tau_{\Theta 0} = bD_0/(2c^2\Delta t) + 0.5$.

Through the Chapman–Enskog procedure [7,35,39,40], macrodynamical Eqs. (4)–(6) can be derived from above evolving equations. For a two-dimensional domain, if the D2Q9 lattice model [25] is chosen for the flow field and the D2Q5 lattice model [7] is chosen for the temperature field, then the present model reduces to the models introduced in Refs. [7,25], and the nonphysical errors in previous models are canceled. The advantages of the present model, such as saving computational resources, have been presented in our previous study [35].

4. Entropy generation

The entropy generation number in turbulent flow is given by [26,41]:

$$S = (\nabla\Theta)^2 + \varphi\left|\overline{\phi}\right|^2 \tag{28}$$

where the irreversibility distribution ratio $\varphi = PrRaEc\Theta_0$ [42], and Ec is the Eckert number [41].

Apparently, it is inconvenient to calculate $|\overline{\phi}|$ (Eq. (17)) directly by conventional numerical methods due to its complex form of spatial derivative [7,43]. However, in the LBM, $|\overline{\phi}|$ can be calculated easily through computing the magnitude of the momentum fluxes Q [7]

$$\left|\overline{\phi}\right| = \frac{3}{2\tau_u\Delta t}\left|Q\right| \tag{29}$$

and Q can be obtained by

$$Q = \sum_k \vec{e}_{k\alpha}\vec{e}_{k\beta}\left(g_k - g_k^{eq}\right) \tag{30}$$

Recognizing the first term in Eq. (28) as reflecting the entropy generation due to thermal diffusion and the second due to viscous dissipation, the entropy generation number can be expressed as

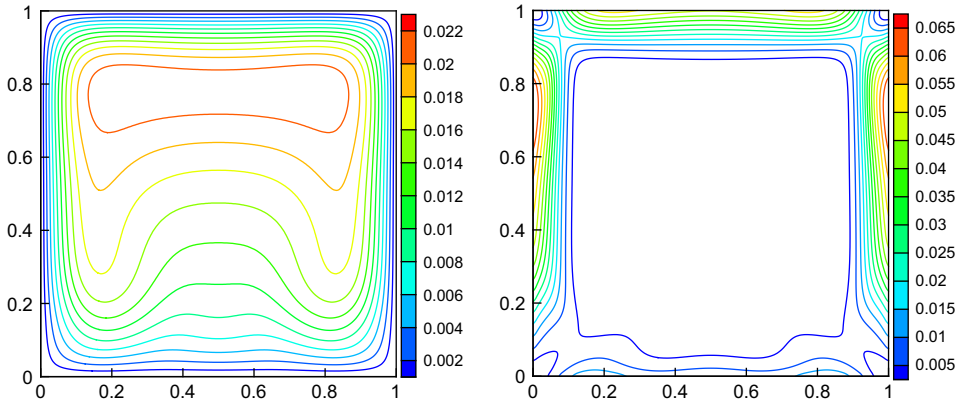

Fig. 7. Isotherms (left) and entropy generation numbers (right) with $Ra = 10^6$, $Pr = 0.6$ and $Ec = 10^{-10}$.

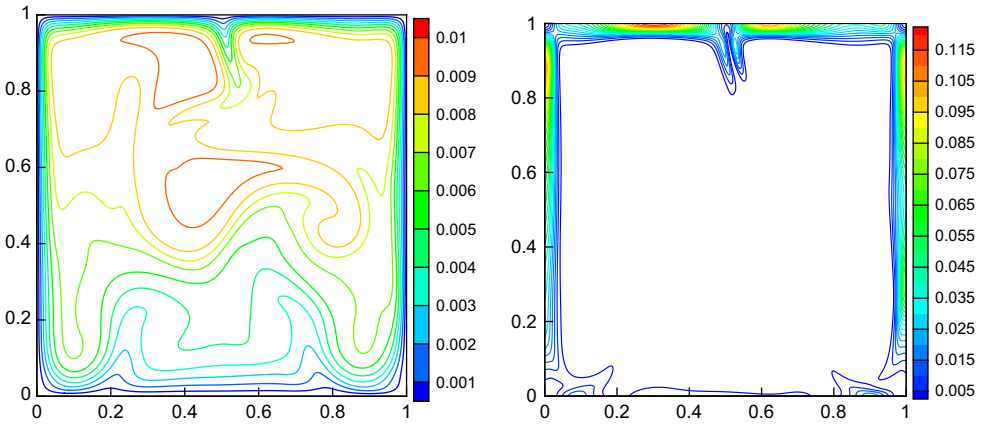

Fig. 8. Isotherms (left) and entropy generation numbers (right) with $Ra = 10^9$, $Pr = 0.6$ and $Ec = 10^{-10}$.

$$S = S_D + S_\mu \tag{31}$$

where the subscripts D and μ are used to indicate the effects of thermal diffusion and viscous dissipation respectively. Usually S_D is referred to as Heat Transfer Irreversibility *HTI* and S_μ as Fluid Friction Irreversibility *FFI* [26]. The Bejan number *Be* is given as [26,42,44]:

$$Be = \frac{S_D}{S} = \frac{HTI}{HTI + FFI} \tag{32}$$

When $Be \gg 0.5$, the irreversibility due to heat transfer dominates, whereas $Be \ll 0.5$ the irreversibility due to viscous effect dominates. When $Be = 0.5$ heat transfer and fluid friction entropy generation are equal.

The total entropy generation number is defined as [26]

$$S_{total} = \int_{\Omega} S \partial\Omega \tag{33}$$

where Ω means the global computational domain.

5. Model validation

In the present study, entropy generation numbers in turbulent natural convection driven by internal heat in a square cavity are investigated for a wide range of *Ra*, *Pr* and *Ec*: $10^6 \le Ra \le 10^{12}$, $0.6 \le Pr \le 6$ and $10^{-10} \le Ec \le 10^{-6}$. The boundary conditions are taken to be $\vec{u} = 0$ and $\Theta = 0$ on all solid walls; the initial conditions are set to be $\vec{u} = 0$; $\Theta = 0$ for all cases. Because the distribution functions at the walls are unknown, the non-equilibrium extrapolation scheme [7] used in our previous studies [45–47] is employed to treat flow and temperature boundary conditions, namely

$$g_k|_w = g_k^{eq}\Big|_w + g_k^{non-eq}\Big|_w = g_k^{eq}\Big|_w + \left(g_k|_f - g_k^{eq}\Big|_f + O\left(\epsilon^2\right)\right) \tag{34}$$

$$f_j\Big|_w = f_j^{eq}\Big|_w + f_j^{non-eq}\Big|_W = f_j^{eq}\Big|_W + \left(f_j\Big|_F - f_j^{eq}\Big|_F + O\left(\epsilon^2\right)\right) \tag{35}$$

where the subscript w and f represent the wall boundary grid and neighbouring fluid grid respectively. ϵ is a small quantity [7].

The D2Q9 and the D2Q5 lattice models are employed to simulate the fluid and thermal distributions respectively, with the grid resolutions 256×256 and 512×512. As Table 1 shows that the grid resolution 256×256 is enough to produce grid-independent numerical results.

Firstly, the numerical simulation was validated by comparing the time-boundary-averaged Nusselt number $Nu_{T,b}$ obtained by the present model with previous data [7,8]. The comparison results are plotted in Figs. 1–3. $Nu_{T,b}$ is defined as [8]

$$Nu_{T,b} = \int_{L_b} \int_{T} Nu(\vec{x}, t) \mathrm{d}t \mathrm{d}\vec{x} \tag{36}$$

It can be found that the present results for $Ra \le 10^{10}$ agree well with those in Refs. [7,8], which verifies and validates the present model. With the increasing of *Ra*, the effect of the eddy viscosity becomes

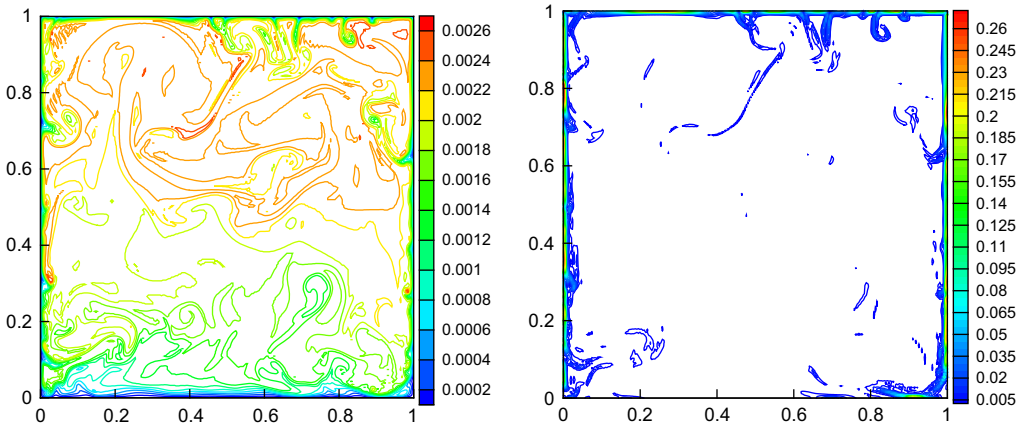

Fig. 9. Isotherms (left) and entropy generation numbers (right) with $Ra = 10^{12}$, $Pr = 0.6$ and $Ec = 10^{-10}$.

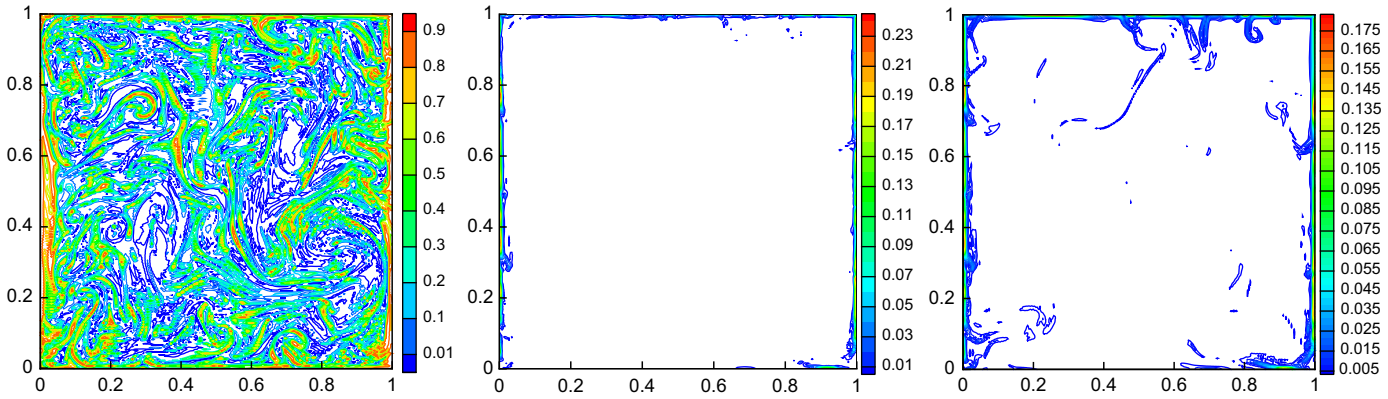

Fig. 10. Maps of Bejan number (left), heat transfer irreversibility (center) and fluid friction irreversibility (right) with $Ra = 10^{12}$, $Pr = 0.6$ and $Ec = 10^{-10}$.

significant so that the deviations of $Nu_{T,\,b}$ between different models on the boundaries set in [7,8].

6. Results and discussions

As Eq. (28) shows, the entropy generation number depends on the Rayleigh number *Ra*, the Prandtl number *Pr* and the Eckert number *Ec*. The behaviors of various results are considered by assuming one of these parameters varying while the others are fixed. Because the flow field becomes unstable when $Ra \geq 10^8$, in the rest part of this paper, if not specified, the instant values, such as the entropy generation number *S*, are measured at time step 7×10^5. At that time the unsteady flows with $Ra \geq 10^8$ are fully developed, namely the stable time-averaged macro-quantities can be measured [7,25].

6.1. Variation in Rayleigh number

As previous studies [26,42,44] pointed out: the characteristics of entropy generation of natural convection flow are dominated by the Rayleigh number *Ra*. Figs. 4 and 5 show the time-volume-averaged Bejan number Be_T, the time-averaged total entropy generation number $S_{total,\,T}$ and the maximum of entropy generation number S_{max} versus various Rayleigh numbers, with fixed values of the Prandtl number $Pr = 0.6$ and the Eckert number $Ec = 10^{-10}$. When $Ra \leq 10^{10}$, the time-volume-averaged Bejan number almost equals one and then decreases quickly against *Ra* increasing. Though the maximum of entropy generation number S_{max} increases quickly with *Ra*, the time-averaged total entropy generation number $S_{total,\,T}$ changes in the opposite trend.

In order to explain these phenomena clearly, three cases $Ra = 10^6$, $Ra = 10^9$ and $Ra = 10^{12}$ are chosen in this subsection, which represent three different states of natural convection due to internal heat generation [7,8]: the steady laminar symmetry ($Ra = 10^6$), the unsteady asymmetric transition ($Ra = 10^9$) and the full turbulence ($Ra = 10^{12}$), as Figs. 6–9 illustrate. When *Ra* is not big enough, the volumetric heat generation is small. Consequently the motion of working fluid due to internal heat generation is quite slow. The entropy generation is mainly caused by heat transfer irreversibility *HTI*, so Be_T approaches one. While $Ra > 10^{10}$, the motion of working fluid is enhanced significantly together with the volumetric heat generation, agreeing with the characteristics of $Nu_{T,\,b}$. Therefore the fluid friction irreversibility *FFI* becomes the domination and $Be \ll 0.5$. It can be seen from Fig. 6 that Be_T tends towards a constant value quickly at the steady laminar symmetric state, whereas for the higher Rayleigh number $Ra = 10^9$, an obvious long-time oscillation of Be_T can be observed before reaching its constant value, and for the full turbulent state Be_T always oscillates around its time-volume-averaged value. The behaviors of the time-averaged entropy generation numbers are identical to that of Be_T. Figs. 7–9 display the maps of temperature distributions and the entropy generation numbers when $Ra = 10^6$, $Ra = 10^9$ and $Ra = 10^{12}$. From these pictures it is obvious that the motion of working fluid is enhanced significantly together with the volumetric heat generation, which makes the distributions of temperature more uniformly and the maximum of temperature smaller. One also can see that in natural convection due to internal heat

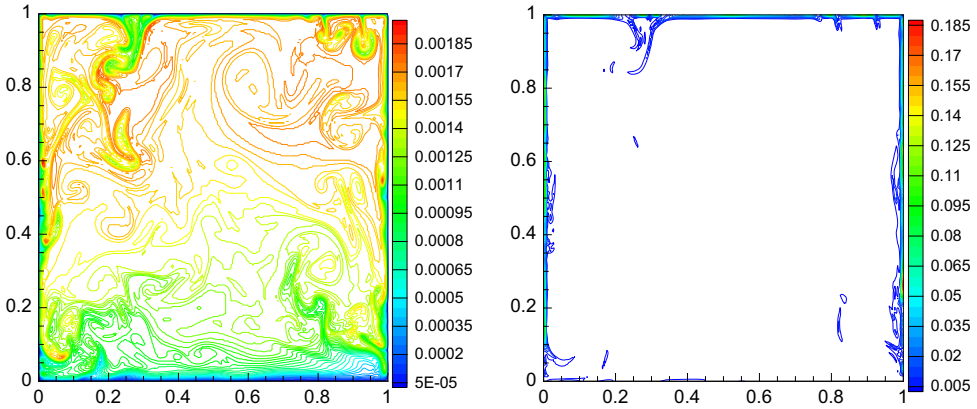

Fig. 11. Isotherms (left) and entropy generation numbers (right) with $Ra = 10^{12}$, $Pr = 2$ and $Ec = 10^{-10}$.

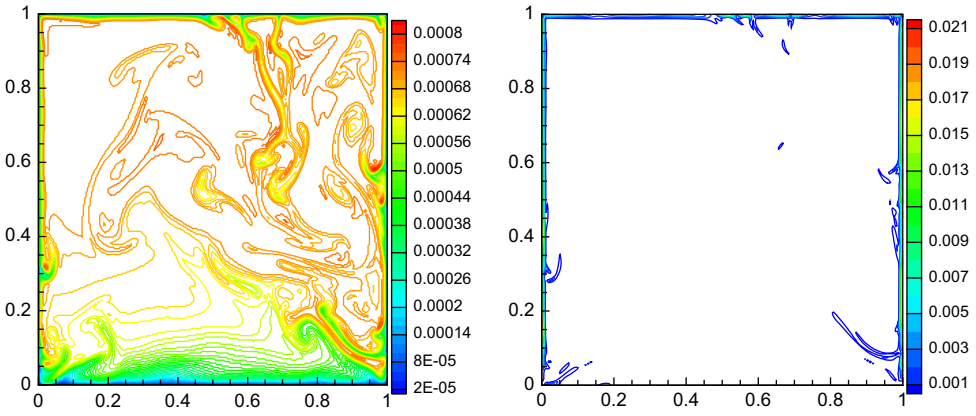

Fig. 12. Isotherms (left) and entropy generation numbers (right) with $Ra = 10^{12}$, $Pr = 6$ and $Ec = 10^{-10}$.

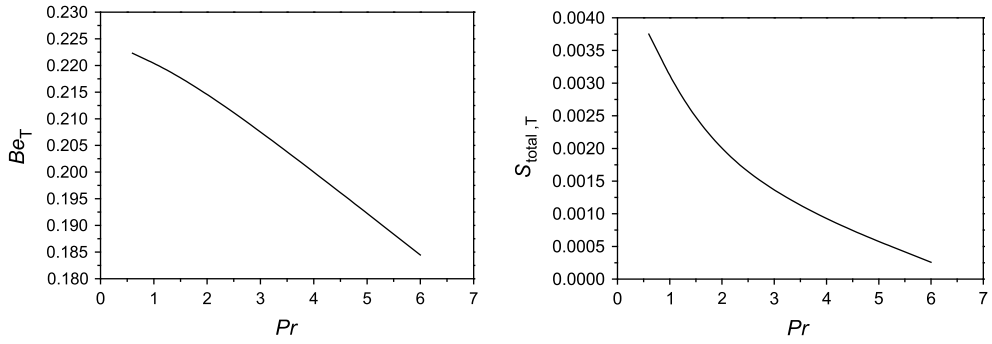

Fig. 13. Time-volume-averaged Bejan number and time-averaged total entropy generation number vs Prandtl number, $Ra = 10^{12}$ and $Ec = 10^{-10}$.

generation, the entropy mainly generates near the boundaries, especially in the vicinity of the top boundary. When *Ra* increases, the small-scale structures become increasing and much finer with the enhancement of motion of working fluid, which make the zone with significant temperature and/or velocity gradients smaller and narrower, confined to the neighborhood of the boundaries. Consequently even though the maximum entropy generation number of higher *Ra* is much bigger than that of lower *Ra*, the time-averaged total entropy generation number of higher *Ra* is fairly smaller than that of lower *Ra* due to the zone with significant entropy generation becomes smaller and narrower when *Ra* increases.

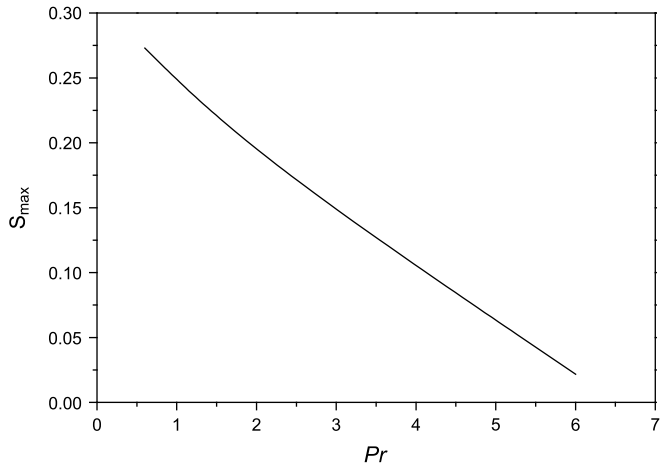

Fig. 14. The maximum of entropy generation number vs Prandtl number, $Ra = 10^{12}$ and $Ec = 10^{-10}$.

Fig. 10 illustrates the maps of the Bejan number, the heat transfer irreversibility and the fluid friction irreversibility when $Ra = 10^{12}$, which typify that of the cases dominated by viscous dissipation. As seen in Fig. 10, over the whole simulation domain except near the boundaries, $Be \ll 0.5$, which indicates that the heat transfer irreversibility is dominative in the vicinity of the boundaries though the inner of the simulation domain is dominated by the fluid friction irreversibility. This phenomenon is caused by the very thin layer with high temperature gradient near the boundaries. Inside the layer the entropy generation due to temperature gradient plays the most important role. As Figs. 9 and 10 show, when $Ra = 10^{12}$, the main features of the maps of the entropy generation number and the fluid friction irreversibility are almost identical, which agree with the result that $Be_T \ll 0.5$ for high *Ra*. For the cases $Ra \leq 10^{10}$, the Bejan number almost equals one not only in the inner of the domain but also in the vicinity of the boundaries. The fluid friction irreversibility can be ignored compared with the heat transfer irreversibility. Therefore we do not show the maps of *Be*, *HTI* and *FFI* for such cases.

6.2. Variation in Prandtl number

To reveal the effect of the Prandtl number *Pr* on entropy generation of natural convection due to internal heat generation, the cases with different values of the Prandtl number $0.6 \leq Pr \leq 6$ but fixed values of the Rayleigh number $Ra = 10^{12}$ and the Eckert number $Ec = 10^{-10}$ are chosen in this subsection, which can typify all cases in this study.

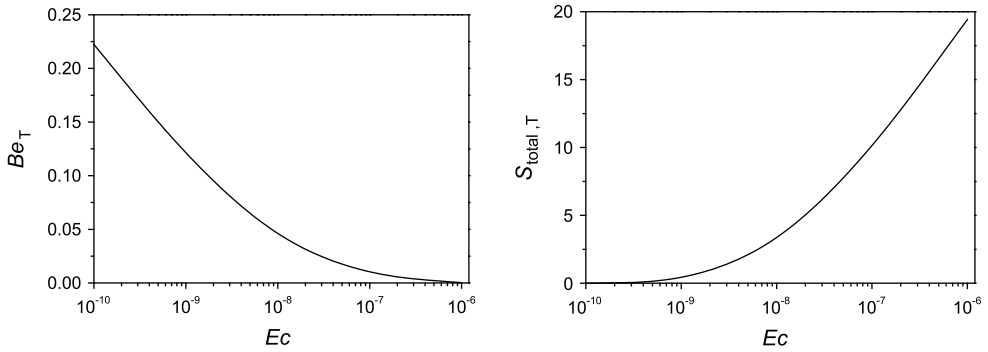

Fig. 15. Time-volume-averaged Bejan number and time-averaged total entropy generation number vs Eckert number, $Ra = 10^{12}$ and $Pr = 0.6$.

Figs. 11 and 12 illustrate the maps of temperature distributions and entropy generation numbers when $Pr = 2$ and $Pr = 6$. From Figs. 9–12, it is clear that the increasing Pr enhances the heat transfer together with the motion of working fluid. The maximum of temperature decreases against Pr increasing. Furthermore, the time-volume-averaged Bejan number, the time-averaged total entropy generation number and the maximum of entropy generation number decrease quickly against Pr increasing, as Figs. 13 and 14 show. Such results are expected according to what mentioned in the above subsection: the enhancement of motion of working fluid makes the distributions of temperature more uniformly and the gradients of velocity smaller, which reduce the time-averaged total entropy generation number and make the heat transfer irreversibility to decrease more quickly than the fluid friction irreversibility.

6.3. Variation in Eckert number

The influence of the Eckert number Ec, which is used to characterize dissipation caused by friction, on entropy generation is straightforward because it only affects the magnitude of the fluid friction irreversibility. Higher Ec means higher FFI. The cases with different values of the Eckert number $10^{-10} \le Ec \le 10^{-6}$ but fixed values of the Rayleigh number $Ra = 10^{12}$ and the Prandtl number $Pr = 0.6$ are chosen in this subsection to clarify such effect.

Figs. 15 and 16 illustrate the time-volume-averaged Bejan number, the time-averaged total entropy generation number and the maximum of entropy generation number versus various Eckert numbers. One can see from these figures that the time-volume-averaged Bejan number approaches zero against Ec increasing, however, the time-averaged entropy generation number and the maximum of entropy generation number increase almost linearly when $Ec > 10^{-8}$, which agree with Eq. (28) because comparing with the fluid friction irreversibility the heat transfer irreversibility is so small that can be ignored when $Ec > 10^{-8}$.

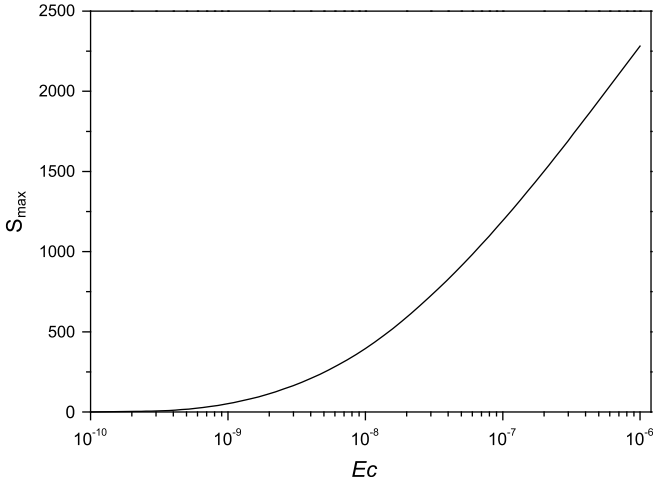

Fig. 16. The maximum of entropy generation number vs Eckert number, $Ra = 10^{12}$ and $Pr = 0.6$.

7. Conclusion

Entropy generation in turbulent natural convection due to internal heat generation was calculated numerically by using an improved lattice Boltzmann model proposed in this study. The influences of the Rayleigh number, the Prandtl number and the Eckert number on entropy generation are evaluated in detail for the first time. It was found that when $Ra \le 10^{10}$, the time-volume-averaged Bejan number almost equals one and then decreases quickly against Ra increasing. Though the maximum of entropy generation number increases quickly with Ra, the time-averaged total entropy generation number changes in the opposite trend. Results showed that for increasing Rayleigh number viscous irreversibility begins to dominate heat transfer irreversibility. Entropy generation is spread over the whole domain at small Rayleigh numbers, but is confined to the neighborhood of the boundaries at high Rayleigh numbers. The numerical results also showed the time-volume-averaged Bejan number, the time-averaged total entropy generation number and the maximum of entropy generation number decrease quickly against Pr increasing. Through this study it was found that the time-averaged total entropy generation number and the maximum of entropy generation number increase almost linearly when $Ec > 10^{-8}$. But the time-volume-averaged Bejan number decreases quickly against Ec increasing.

Acknowledgments

This work was partially supported by the Alexander von Humboldt Foundation, Germany. The authors gratefully acknowledges Prof. B.C. Shi and Dr. H.J. Liu in the Huazhong University of Science and Technology, China for their helpful discussion and sharing the C++ code of the lattice-BGK model.

References

[1] Y. Tasaka, Y. Takeda, Effects of heat source distribution on natural convection induced by internal heating, Int. J. Heat Mass Transfer 48 (2005) 1164–1174.
[2] F.A. Kulacki, D.E. Richards, Natural convection in plane layers and cavities with volumetric energy sources, in: S. Kakac, W. Aung, R. Viskanta (Eds.), Natural Convection-Fundamentals and Applications, Hemisphere (1985), pp. 179–254 New York.
[3] D.P. Mckenzie, J.M. Roberts, N.O. Weiss, Convection in the earth's mantle: toward a numerical simulation, J. Fluid Mech. 62 (1974) 465–538.

[4] B. Travis, S. Weinstein, P. Olson, Three-dimensional convection planforms with internal heat generation, Geophys. Res. Lett. 17 (1990) 243–246.
[5] A. Sharmaa, K. Velusamya, C. Balajib, Conjugate transient natural convection in a cylindrical enclosure with internal volumetric heat generation. Ann. Nucl. Energ. doi:10.1016/j.anucene.2008.01.008.
[6] S.D. Lee, J.K. Lee, K.Y. Suh, Natural convection thermo fluid dynamics in a volumetrically heated rectangular pool, Nucl. Eng. Des. 237 (2007) 473–483.
[7] H.J. Liu, C. Zou, B.C. Shi, et al., Thermal lattice-BGK model based on large-eddy simulation of turbulent natural convection due to internal heat generation, Int. J. Heat Mass Transfer 49 (2006) 4672–4680.
[8] A. Horvat, I. Kljenak, J. Marn, Two-dimensional large-eddy simulation of turbulent natural convection due to internal heat generation, Int. J. Heat Mass Transfer 44 (2001) 3985–3995.
[9] R.R. Nourgaliev, T.N. Dinh, B.R. Sehgal, Effect of fluid Prandtl number on heat transfer characteristics in internally heated liquid pools with Rayleigh numbers up to 10^{12}, Nucl. Eng. Des. 169 (1997) 165–184.
[10] F.A. Kulacki, R.J. Goldstein, Thermal convection in a horizontal fluid layer with uniform voumetric energy sources, J. Fluid Mech. 55 (1972) 271–287.
[11] F.A. Kulacki, M.E. Nagle, Natural convection in a horizontal fluid layer with volumetric energy sources, J. Heat Transfer 97 (1975) 204–211.
[12] F.J. Asfia, B. Frantz, V.K. Dhir, Experimental investigation of natural convection heat transfer in spherical segments, J. Heat Transfer 118 (1996) 31–37.
[13] T.N. Dinh, R.R. Nourgaliev, Turbulence modeling for large volumetrically heated liquid pools, Nucl. Eng. Des. 169 (1997) 131–150.
[14] M. Wörner, M. Schmidt, G. Grötzbach, Direct numerical simulation of turbulence in an internally heated convective fluid layer and implications for statistical modelling, J. Hydraul. Res. 35 (1997) 773–797.
[15] R. Benzi, S. Succi, M. Vergassola, The lattice Boltzmann equation: theory and applications, Phys. Rep. 222 (1992) 145–197.
[16] S. Chen, G.D. Doolen, Lattice Boltzmann method for fluid flows, Annu. Rev. Fluid Mech. 30 (1998) 329–364.
[17] S. Succi, The Lattice Boltzmann Equation for Fluid Dynamics and Beyond, Oxford University Press, Oxford, 2001.
[18] R.J. Goldstein, W.E. Ibele, S.V. Patankar, et al., Heat transfer-a review of 2003 literature, Int. J. Heat Mass Transfer 49 (2006) 451–534.
[19] D.O. Martinez, W.H. Matthaeus, S. Chen, et al., Comparison of spectral method and lattice Boltzmann simulations of two-dimensional hydrodynamics, Phys. Fluid. 6 (1994) 1285–1298.
[20] X. He, G.D. Doolen, T. Clark, Comparison of the lattice Boltzmann method and the artificial compressibility method for Navier–Stokes equations, J. Comput. Phys. 179 (2002) 439–451.
[21] Y.Y. Al-Jahmany, G. Brenner, P.O. Brunn, Comparative study of lattice-Boltzmann and finite volume methods for the simulation of laminar flow through a 4:1 planar contraction, Int. J. Numer. Meth. Fluid. 46 (2004) 903–920.
[22] A. Al-Zoubi, G. Brenner, Comparative study of thermal flows with different finite volume and lattice Boltzmann schemes, Int. J. Mod. Phys. C 15 (2004) 307–319.
[23] T. Seta, E. Takegoshi, K. Okui, Lattice Boltzmann simulation of natural convection in porous media, Math. Comput. Simulat. 72 (2006) 195–200.
[24] S. Chen, Z.H. Liu, Z. He, et al., A new numerical approach for fire simulation, Int. J. Mod. Phys. C 18 (2007) 187–202.
[25] B.C. Shi, Z.L. Guo, Thermal lattice BGK simulation of turbulent natural convection due to internal heat generation, Int. J. Mod. Phys. B 9 (2002) 48–51.
[26] A. Bejan, Entropy Generation Through Heat and Fluid Flow, second ed. Wiley, New York, 1994.
[27] A. Bejan, Entropy Generation Minimization, CRC Press, Boca Raton, FL, 1996.
[28] A. Bejan, Shape and Structure from Engineering to Nature, Cambridge University Press, New York, 2000.
[29] M. Magherbi, N. Hidouri, H. Abbassi, A. Brahim, Influence of Dufour effect on entropy generation in double diffusive convection, Int. J. Exergy 4 (2007) 227–252.
[30] Y. Varol, H. Oztop, A. Koca, Entropy production due to free convection in partially heated isosceles triangular enclosures, Appl. Therm. Eng. 28 (2008) 1502–1513.
[31] K. Hooman, A. Ejlali, F. Hooman, Entropy generation analysis of thermally developing forced convection in fluid-saturated porous medium, Appl. Math. Mech. Engl. Ed. 29 (2008) 169–177.
[32] A. Baytas, Entropy generation for thermal nonequilibrium natural convection with a non-Darcy flow model in a porous enclosure filled with a heat-generating solid phase, J. Porous Media 10 (2007) 261–275.
[33] A. Baytas, Optimization in an inclined enclosure for minimum entropy generation in natural convection, J. Non-equilibrium Thermody 22 (1997) 145–155.
[34] K. Hooman, F. Hooman, S. Mohebpour, Entropy generation for forced convection in a porous channel with isoflux or isothermal walls, Int. J. Exergy 5 (2008) 78–96.
[35] S. Chen, Z. Liu, C. Zhang, et al., A novel coupled lattice Boltzmann model for low Mach number combustion simulation, Appl. Math. Comput. 193 (2007) 266–284.
[36] Z. Guo, C. Zheng, B. Shi, Discrete lattice effects on the forcing term in the lattice Boltzmann method, Phys. Rev. E 65 (2002) 046308/1–046308/6.
[37] S. Chen, Z. Liu, B. Shi, et al., Computation of gas-solid flows by finite difference Boltzmann equation, Appl. Math. Comput. 173 (2006) 33–49.
[38] S. Chen, Z.H. Liu, B.C. Shi, et al., A novel incompressible finite-difference lattice Boltzmann equation for particle-laden flow, Acta Mech. Sin. 21 (2005) 574–581.
[39] Z.L. Guo, B.C. Shi, C.G. Zheng, A coupled lattice BGK model for the Boussinesq equations, Int. J. Numer. Meth. Fluid. 39 (2002) 325–342.
[40] B.C. Shi, N. He, N. Wang, A unified thermal lattice BGK model for Boussinesq equations, Prog. Comput. Fluid Dyn. 5 (2005) 50–64.
[41] Y. Ji, K.O. Homan, Transition from gravity-to inertia-dominated behavior computed for the turbulent stably-stratified filling of an open enclosure, Int. J. Heat Fluid Flow 27 (2006) 490–501.
[42] M. Magherbi, H. Abbassi, A.B. Brahim, Entropy generation at the onset of natural convection, Int. J. Heat Mass transfer 46 (2003) 3441–3450.
[43] T.J. Chung, Computational Fluid Dynamics, Cambridge University Press, Cambridge, 2002.
[44] M. Famouri, K. Hooman, Entropy generation for natural convection by heated partitions in a cavity, Int. Comm. Heat Mass Transfer 35 (2008) 492–502.
[45] S. Chen, J. Tolke, M. Krafczyk, A new method for the numerical solution of vorticity-streamfunction formulations, Comput. Meth. Appl. Mech. Eng. 198 (2008) 367–376.
[46] S. Chen, J. Tolke, S. Geller, M. Krafczyk, Lattice Boltzmann model for incompressible axisymmetric flows, Phys. Rev. E 78 (2008) 046703.
[47] S. Chen, J. Tolke, M. Krafczyk, Simulation of buoyancy-driven flows in a vertical cylinder using a simple lattice Boltzmann model, Phys. Rev. E 79 (2009) 016704.